




Cite this: *RSC Adv.*, 2019, 9, 20941

# Removal of Hg(II) in aqueous solutions through physical and chemical adsorption principles

Mengdan Xia,<sup>a</sup> Zhixin Chen,<sup>b</sup> Yao Li,<sup>a</sup> Chuanhua Li,<sup>c</sup> Nasir M. Ahmad,<sup>d</sup> Waqas A. Cheema<sup>d</sup> and Shenmin Zhu \*<sup>a</sup>

Adsorption has been the focus of research on the treatment of heavy metal mercury pollution since it is among the most toxic heavy metals in existence. The US EPA has set a mandatory discharge limit of 10  $\mu\text{g Hg L}^{-1}$  for wastewater and for drinking water a maximum accepted concentration of 1  $\mu\text{g Hg L}^{-1}$ . Physical adsorption and chemical adsorption are the two major mechanisms of adsorption methods used for mercury removal in aqueous sources. The recent decades' research progress is reviewed to elaborate varieties of adsorption materials ranging from materials with large surface area for physical adsorption to metal oxides for chemical adsorption. Many examples are presented to illustrate the adsorption principles and clarify the relationship between the structure and performance of the adsorbents. The combination of physical adsorption and chemical adsorption gives rise to numbers of potential mercury removal composites. This review demonstrates the adsorption mechanism and the performance of varieties of adsorbents, which would provide a comprehensive understanding on the design and fabrication of new materials for the removal of heavy metal ions in water.

Received 13th March 2019

Accepted 20th June 2019

DOI: 10.1039/c9ra01924c

[rsc.li/rsc-advances](http://rsc.li/rsc-advances)

## 1. Introduction

With the development of human civilization, the conflict between industrialization and environmental pollution has become a serious issue and needs to be addressed in modern society.<sup>1</sup> One of the pollutions is heavy metal ion pollution. Mercury is a major toxic element found in wastewater in the environment.<sup>2</sup> As a dominant constituent of environmental inorganic mercury, Hg(II) can combine with the cysteine of human protein. Through sulfate methylation, Hg(II) converts into CH<sub>3</sub>Hg – a major organic mercury causing high bio-accumulation in food chains.<sup>3–5</sup> Serious damage has been

<sup>a</sup>State Key Laboratory of Metal Matrix Composites, Shanghai Jiao Tong University, Shanghai 200240, PR China. E-mail: smzhu@sjtu.edu.cn; Fax: +86 21 3420 2749; Tel: +86 21 3420 2584

<sup>b</sup>Engineering Materials Institute, School of Mechanical, Materials & Mechatronics Engineering, University of Wollongong, Wollongong, 2522, Australia

<sup>c</sup>Shanghai Solid Waste Disposal Co. Ltd, Shanghai, PR China

<sup>d</sup>Polymer Research Lab, School of Chemical and Materials Engineering (SCME), National University of Sciences and Technology (NUST), H-12 Sector, Islamabad-44000, Pakistan



Miss Mengdan Xia received her Bachelor degree in Chemical Science from the Shanghai Jiao Tong University, China in 2017. She is presently a postgraduate student at the School of Materials Science and Engineering in Shanghai Jiao Tong University, under the supervision of Prof. Shenmin Zhu. She is currently working on research of hierarchically structured porous carbon nanocomposite and

functional polymer membrane, as well as their application on water treatment.



Dr Yao Li received his PhD in Material Science from the Shanghai Jiao Tong University, China in 2015 under the supervision of Prof. Di Zhang and Prof. Shenmin Zhu. He joined as a research associate at Shanghai Jiao Tong University at 2015. He is working on research of bio-inspired material and carbon matrix material, as well as their application on environment treatment and energy storage.



reported in the brain, heart, liver and kidneys as well as nervous and metabolic systems, and it even leads to cancer.<sup>6</sup> The gathering effect of food chains would increase the mercury concentration in water by 1000 times with straightforward delivery into the human body.<sup>7</sup>

Nowadays it is mandatory to reduce Hg(II) concentration to 0.001–0.002 mg L<sup>-1</sup> in wastewater prior to discharge into the environment.<sup>8</sup> The upper limit of mercury in wastewater is set as 0.001 mg L<sup>-1</sup> in China (DB12 356-2018), and in the US it is 0.001 mg L<sup>-1</sup> according to the national primary drinking water regulations.<sup>9,10</sup>

To deal with the increasingly serious mercury pollution, many methods have been investigated for the removal of Hg(II), including chemical precipitation, ion exchange, solvent extraction, ultrafiltration and adsorption.<sup>11–15</sup> The chemical precipitation method requires hazardous chemical reagents and a long time. Ion exchange has a specific ability to exchange its cations with the metals in the wastewater, but it is inefficient and can cause secondary pollution. The solvent extraction method consumes large quantities of solvent and is limited by poor selectivity. Ultrafiltration is a membrane technique working at low transmembrane pressures, limited by fouling issues and high cost.

On the other hand, adsorption is considered as the most promising technique due to its simplicity, selectivity, high efficiency, low cost, and operational convenience.<sup>16</sup> The adsorption method refers to separating pollutants from wastewater through the interaction between the adsorbents and pollutants.<sup>17</sup> The interaction between the adsorbents and pollutants is commonly divided into physical adsorption and chemical adsorption according to the adsorption mechanism. Physical adsorption usually involves facile fabrication but suffers from relatively low adsorption capacity. Chemical adsorption has the advantage of high efficiency but also has problems with secondary pollution.

The traditional adsorbents which involve a single adsorption way, such as marine macroalga, goethite and bentonite, are suffering from low adsorption capacities and low removal efficiencies of Hg(II). Hence, researchers continue to seek new efficient adsorbents. Among these, the current trend for Hg(II) removal is to combine the advantage of physical adsorption and

chemical adsorption, based on hierarchical structure.<sup>18,19</sup> To date, many adsorbents of Hg(II) have been examined. New developed adsorbents, including activated carbon, silica, hydroxyapatite, multiwalled carbon nanotubes (MWCNTs), two-dimensional metal carbides and many different kinds of polymers *etc.*<sup>20–22</sup> were demonstrated to be effective for Hg(II) removal. Hierarchical structured porous material, such as porous carbon fabricated from bio-species is of great interests owing to interconnected three-dimensional pore structures, high specific surface area and surface modifiability. Magnetic modified porous composites with fine pore structure are promising candidates for adsorption and show dramatically improved adsorption performance. Hierarchical porosity often provides full accessibility of narrow cavities and efficient mass transport property. Bioinspired carbide-derived carbons with hierarchical pore structure were developed by C. Fischer *et al.* for the adsorption of Hg(II).<sup>21</sup> The micropore size of bioinspired carbons can be adjusted with a high accuracy to enhance the adsorption performance. Additionally, some novel materials with two-dimensional nanofiber structure also provide unique approach for heavy metal removal. Two-dimensional (2D) metal carbides (MXenes) such as Ti<sub>3</sub>C<sub>2</sub>T<sub>x</sub>, and nanofiber material such as CNT are promising candidates for Hg(II) adsorption.<sup>22</sup> Generally, one adsorbent material may involve one or more adsorption mechanisms.

According to US Environmental Protection Agency (EPA), mercury has a low limit of 0.01 mg L<sup>-1</sup> for hazardous waste. It clearly indicated the stringent environmental remediation for Hg(II) to be substantially removed from the aqueous sources before being discharged. This review critically analyzes earlier research work in area of Hg(II) removal from aqueous sources using physical and chemical adsorption techniques, and highlights the relationships between the structure and performance of adsorbents. In addition, elaboration of specific adsorption materials corresponding to different adsorption mechanisms and their principle is illustrated in details.

## 2. Adsorption method for Hg(II) removal

### 2.1. Physical adsorption for Hg(II) removal

Utilizing the large surface area of adsorbent particles, a physical adsorption process involves van der Waals interaction or electrostatic interaction between the adsorbent and Hg(II).<sup>23</sup> Porous structured materials can remove Hg(II) from aqueous solution mainly through physical adsorption, such as activated carbon, mesoporous silica and zeolite. Porous structured materials are generally prepared from various agricultural waste and plant residues such as bagasse, silk cotton hull, coconut tree sawdust, maize cob, peanut hull, wood dust and coir pith *etc.*<sup>24</sup> Thus, the adsorbents that adopt physical adsorption are usually easy to develop and can also be made eco-friendly.

As early as 1966 Fornwalt *et al.* purified liquids by activated carbon through physical adsorption.<sup>25</sup> Since then various forms of carbon-based materials have been developed to remove metal ions. Skodras *et al.* prepared activated carbon by using



*Prof. Shenmin Zhu received her PhD degree from Shanghai Jiao Tong University in 2001. She is presently a professor at the School of Materials Science and Engineering, State Key Lab of Metal Matrix Composites, Shanghai Jiao Tong University. Her current fields of interest are graphene-based functional materials, porous carbon, and bio-inspired photonic crystals with stimuli-responsive properties.*



agricultural residues and waste tires, and studied Hg(II) removal through physical adsorption.<sup>26</sup> Fig. 1 displays the nitrogen and carbon dioxide adsorption isotherms for the as-prepared activated carbon to demonstrate the relationships between the surface area and adsorption behaviors. The carbon produced from olive seed has the BET surface area of  $1690 \text{ m}^2 \text{ g}^{-1}$  and the high mercury adsorption capacity of  $869 \mu\text{g g}^{-1}$ . Large BET surface area and total micropore volume were found to promote mercury adsorption capacity. This indicates that large surface area and an efficient micropore structure would provide necessary space and sites for physical adsorption of mercury to further optimize the adsorption capacity (Table 1).

M. Zabihi *et al.* fabricated porous carbons with surface area of  $780 \text{ m}^2 \text{ g}^{-1}$  from walnut shells, which exhibited a high monolayer adsorption capacity of  $151.5 \text{ mg g}^{-1}$  for Hg(II) removal.<sup>27</sup> Zhang *et al.* studied various activated carbons extracted from organic sewage sludge (SS) *via* variety kinds of chemical activation.<sup>28</sup> Of these,  $\text{ZnCl}_2$  activated carbon exhibited the highest adsorption capacity, and approximately 60 to 80% of the Hg(II) adsorbed by activated carbon could be recovered *via* sonication. Owing to the chemical activation by  $\text{ZnCl}_2$ , comprehensive properties of the activated carbon were dramatically enhanced. The effect of adsorbent dosage on the Hg(II) adsorption efficiency was studied in Fig. 2. Apparently, the percentage of Hg(II) removal increased with the increase of the adsorbent dosage. It is noticed that more dosage of the activated carbons offered more active sites for Hg(II) to anchor on.

Except carbon materials, zeolites and silica also possess abundant pore channels and can be also promising adsorbents for Hg(II) through physical adsorption. Sedigheh *et al.* synthesized hierarchical nanoporous ZSM-5 zeolite from bagasse using for Hg(II) removal.<sup>29</sup> Silica powder was used in the synthesis of adsorbent. Hierarchical zeolites demonstrated excellent adsorption efficiency of 96.3% due to their unique surface to overcome the diffusion and mass transport limitation of micropores and active sites posited within interface.<sup>30,31</sup> Several other studies have been also devoted to the adsorbents

with fine porous structure and high surface area, such as magnetic mesoporous silicas,<sup>32</sup> regenerable multifunctional mesoporous silica,<sup>33</sup> magnetic self-assembled zeolite clusters,<sup>34</sup> multi-walled carbon nanotubes<sup>35</sup> and LTA nanozeolite.<sup>36</sup>

The adsorption kinetics and isotherms mechanism of Hg(II) adsorption are interpreted by the following example, as presented in Fig. 3. In one of recent work by our group, a hierarchically structured carbon-based materials derived from bagasse was fabricated for Hg(II) adsorption.<sup>37</sup> The maximum Hg(II) removal efficiency of 96.8% was achieved at equilibrium.

Commonly, pseudo-first order model and pseudo-second order model are applied to simulate the kinetics data of Hg(II) adsorption, expressed as eqn (1) and (2) in the Table 2. Where  $q_e$  and  $q$  correspond to the adsorption capacities at equilibrium and time  $t$  (min) respectively;  $K_1$  and  $K_2$  are the sorption rate constants; and  $R^2$  is the resultant fitting parameter. Fig. 3(a) adopted pseudo-second order model ( $R^2 = 0.999$ ) to describe the adsorption kinetics, which fitted well with the experimental ones, suggesting that the rate limiting step was the adsorption process instead of the diffusion process.<sup>38</sup>

Adsorption isotherms in Fig. 3(b) describes the amount of Hg adsorbed by unit mass adsorbent at constant temperature as a function of Hg(II) concentration at equilibration. The Langmuir isotherm model was applied for monolayer adsorption with all binding sites equal.<sup>39</sup>

The Freundlich isotherm model described multilayer adsorption on a heterogeneous surface.<sup>40</sup> Equations of two models are given as eqn (3) and (4) in Table 2, where  $C_e$  is the equilibration concentration of Hg;  $q_{\text{max}}$  is the maximum adsorption capacity;  $K_L$  and  $K_F$  are Langmuir and Freundlich constants;  $1/n$  is the constant related to adsorption intensity. The curves in Fig. 3(b) are fitting well with Freundlich isotherm model ( $R^2 = 0.989$ ), suggesting the heterogeneity of the porous carbons. Physical adsorption is consistent with multilayer adsorption because of its space limitation.

Activated carbon fiber (ACF) was developed with optimize morphology based on activated carbon. Its strong mechanical property, large surface area and fine pore structure bring the

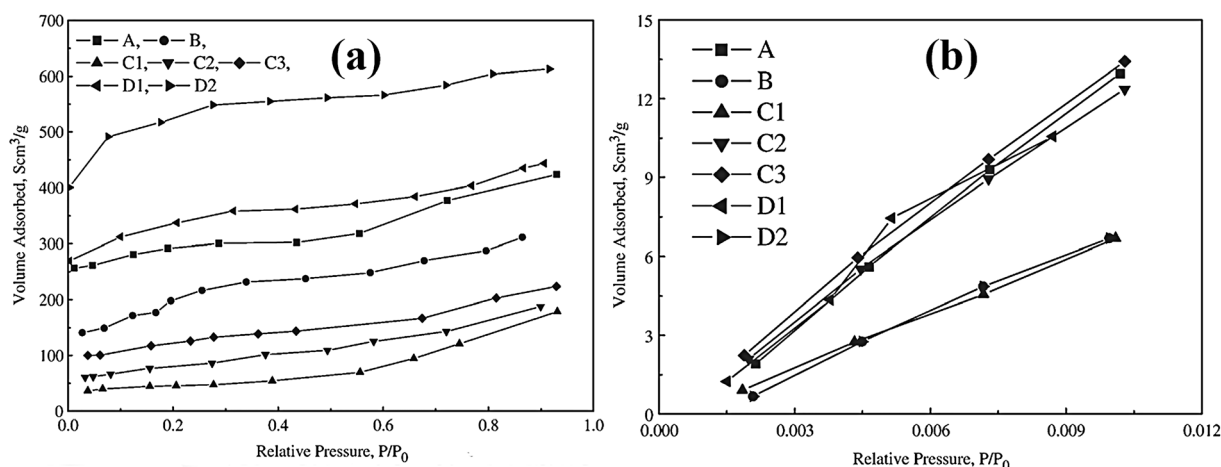


Fig. 1  $\text{N}_2$  and  $\text{CO}_2$  adsorption isotherms of the activated carbon produced from different starting materials.<sup>26</sup> This figure has been adapted from ref. 26 with permission from Elsevier.



Table 1 Activated carbons A, B, C1, C2, C3, D1 and D2 produced under different conditions<sup>26</sup>

Raw material	Pine wood	Oak wood	Waste tires			Olive seed waste	
Activated carbon	A	B	C1	C2	C3	D1	D2
Pyrolysis conditions (°C, h)	800/0.75		800/0.75			800/1	
Chemical treatment	—		—			KOH	
Activating gas/flow rate (cm <sup>3</sup> min <sup>-1</sup> )	H <sub>2</sub> O–CO <sub>2</sub> /758 × 10 <sup>3</sup>		H <sub>2</sub> O–CO <sub>2</sub> /758 × 10 <sup>3</sup>			N <sub>2</sub> /100	
Activating conditions (°C, h)	900/2.5		900/0.5	900/1	900/2	800/1	800/3

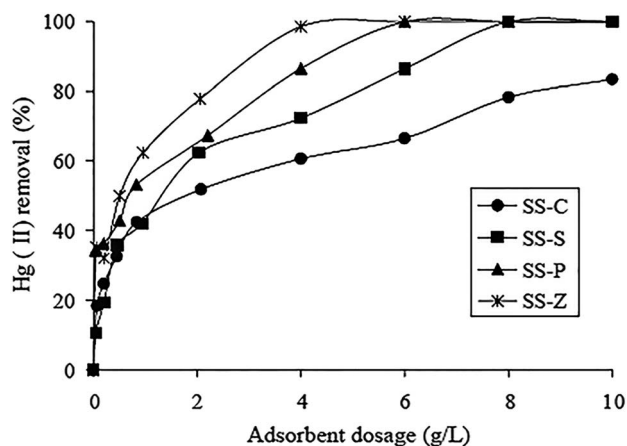


Fig. 2 Effect of adsorbent dosage on Hg(II) removal. (Hg<sup>2+</sup> 200 mg L<sup>-1</sup>, pH 5.0, time 7 h, 25 °C.) SS-S, SS-P, SS-Z and SS-C represented activated carbons treated by H<sub>2</sub>SO<sub>4</sub>, H<sub>3</sub>PO<sub>4</sub>, ZnCl<sub>2</sub> and that with no treatment.<sup>28</sup> This figure has been adapted from ref. 28 with permission from Elsevier.

advantage of fast adsorption. Nabais *et al.* prepared ACF from a commercial acrylic textile fiber for the removal of mercury from aqueous solution and from flue gases.<sup>41</sup> The ACF samples displayed quite large BET surface area range of 848–1259 m<sup>2</sup> g<sup>-1</sup> and could remove HgCl<sub>2</sub> from aqueous within the range of 290–710 mg g<sup>-1</sup>. Carbon nanotube (CNT), also has great prospect for heavy metal Hg(II) removal. Its unique carbon atom hexagon array and  $\pi$ - $\pi$  interaction offer large numbers of physical adsorption sites for Hg(II).<sup>42,43</sup> Aerogels materials, in addition, can give assistance to physical adsorption through 3D cross-linking structured network.<sup>44</sup>

Porous structured materials are ideal candidates for heavy metal Hg(II) removal because they have large surface area and fine pore structure. The pore channels offer large numbers of physical adsorption sites for Hg(II). Hierarchically adsorbents are often easy to synthesize and possess considerable surface area and adsorption capacity. Nevertheless, pure porous materials work through physical adsorption only, which may be disadvantaged by relatively long interaction period, low adsorption capacity and the challenging recovery process of adsorbents.<sup>45,46</sup>

## 2.2. Chemical adsorption for Hg(II) removal

In chemical adsorption, adsorbents react with the contaminant or have chemical complexation effects with the contaminant.<sup>47</sup> The adsorbents that remove Hg(II) in aqueous through chemical adsorption include inorganic active matters and organics. Inorganic active matters are generally metal oxides or metal oxide composites. Metal oxides possess a strong binding affinity with Hg(II) cations or molecules, and offer plentiful active adsorption sites for Hg(II) *via* coordination through oxygen atoms. Organic adsorbents involve macromolecules, functional group chains and proteins (cysteine) *etc.*<sup>48,49</sup> As compared with physical adsorption, chemical adsorption often has a faster removal rate and higher removal efficiency on trace Hg(II). Some magnetic chemical adsorbents can be recovered from the pollutant through magnetic separation for reuse and recycling.<sup>50</sup>

Naturally abundant metal oxides such as iron oxide and manganese oxide exhibit outstanding performance in Hg(II) chemical adsorption. One of the mechanisms of the common chemical adsorption is through oxidation–redox reaction.<sup>51</sup>

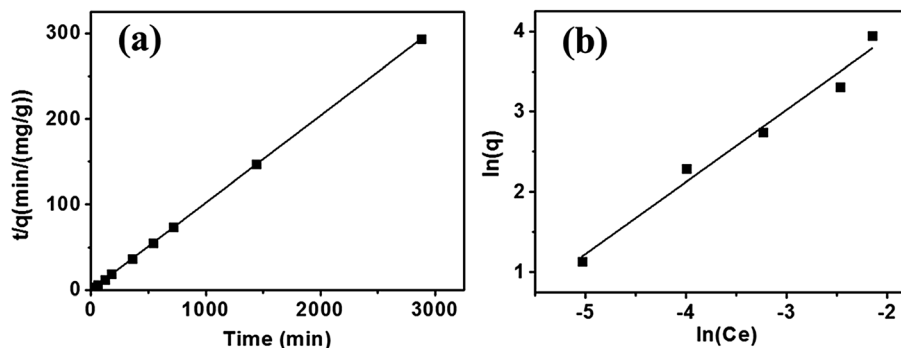


Fig. 3 (a) Pseudo-second order model for Hg sorption (pH 6, adsorbent 80 mg L<sup>-1</sup>, Hg<sup>2+</sup> 1.0 mg L<sup>-1</sup>, 25 ± 2 °C). (b) Freundlich isotherm model for Hg sorption (Hg<sup>2+</sup> 0.5–5.0 mg L<sup>-1</sup>, pH 6, adsorbent 80 mg L<sup>-1</sup>, time 24 h, 25 ± 2 °C).<sup>37</sup> This figure has been adapted from ref. 37 with permission from Elsevier.





Table 2 The kinetics and isotherms parameters, and the correlation coefficients,  $R^{2a}$ 

Pseudo-first order constants			Pseudo-second order constants		
$\ln(q_e - q) = \ln q_e - K_1 t$ (1)			$t/q = 1/(K_2 q_e^2) + t/q_e$ (2)		
$q_e$ (mg g <sup>-1</sup> )	$K_1$ (g mg <sup>-1</sup> min <sup>-1</sup> )	$R^2$	$q_e$ (mg g <sup>-1</sup> )	$K_2$ (g mg <sup>-1</sup> min <sup>-1</sup> )	$R^2$
9.8	0.005	0.944	9.8	0.083	0.999
Langmuir constants			Freundlich constants		
$\frac{C_e}{q_e} = \frac{1}{K_L q_{max}} + \frac{C_e}{q_{max}}$ (3)			$\ln q_e = \ln K_F + \frac{1}{n} \ln C_e$ (4)		
$q_{max}$ (mg g <sup>-1</sup> )	$K_L$ (L mg <sup>-1</sup> )	$R^2$	$1/n$	$K_F$ (L g <sup>-1</sup> )	$R^2$
51.8	9.280	0.502	0.898	304.3	0.989

<sup>a</sup> Where  $q_e$ ,  $q_{max}$ ,  $K_1$ ,  $K_2$ ,  $1/n$ ,  $K_L$ ,  $K_F$  are defined by eqn (1)–(4), respectively.

Some metal oxides possess reducibility on Hg(II), such as MnO<sub>2</sub>. Ma *et al.* evaluated the effectiveness of *in situ* MnO<sub>2</sub> on Hg(II) removal. Their results suggested that the reducing properties of MnO<sub>2</sub> significantly enhanced flocculation and improved the performance of Hg(II) removal.<sup>52</sup> Metal oxide composites exhibit higher adsorption efficiency than single metal oxides. Metal oxides often coexist in soil and water and easily form mixed oxides.<sup>53</sup> Binary oxides with surface charge and variable valence elements have higher surface activities than single oxides and can take advantage of both unique properties of them.<sup>54</sup> Ali *et al.* studied the adsorption capacities of binary oxides and found that nanoparticles containing silver and zinc had better performance than single silver or zinc oxide.<sup>55</sup> Fe, Mn, Zn and Ag oxides, for their high surface activity and modifiability, are promised to be the new generation of environmental remediation materials.

The reaction mechanism of chemical adsorption by metal hydroxide composite is generally involved in complexation–flocculation. Lu *et al.* investigated the removal of trace Hg(II) in aqueous by manganese–ferric hydroxide (*in situ* formed).<sup>56</sup> The Mn–Fe oxide was fabricated by reacting KMnO<sub>4</sub> with Fe(II) in simulated natural water. The mercury in the experimental solution existed mainly in the non-charged forms, including

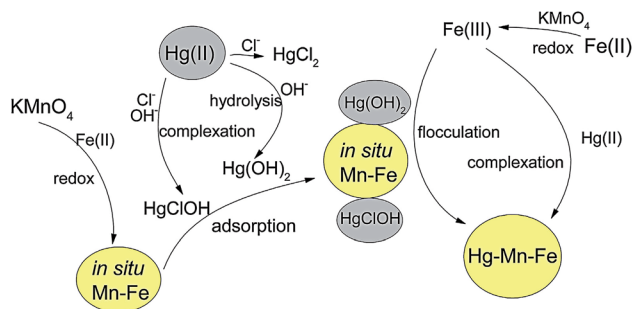


Fig. 4 Schematic diagram of the mechanisms of Hg(II) removal by *in situ* Mn–Fe.<sup>55</sup> This figure has been adapted from ref. 55 with permission from Elsevier.

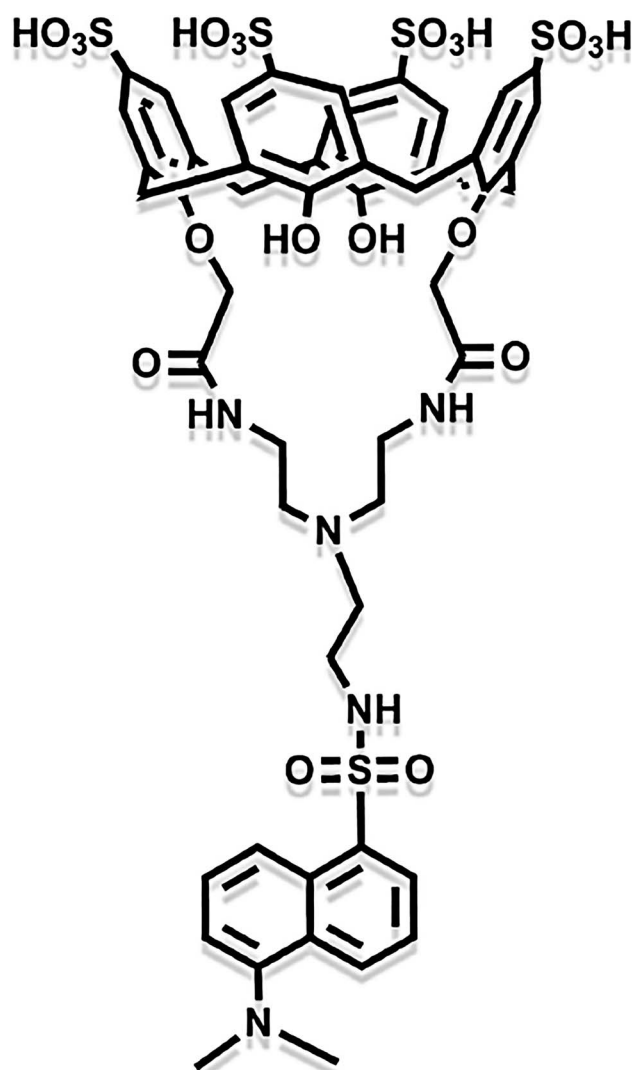


Fig. 5 The molecule structure of the coated calixarene in the nuclear–shell hybrid.<sup>61</sup> This figure has been adapted from ref. 61 with permission from Elsevier.



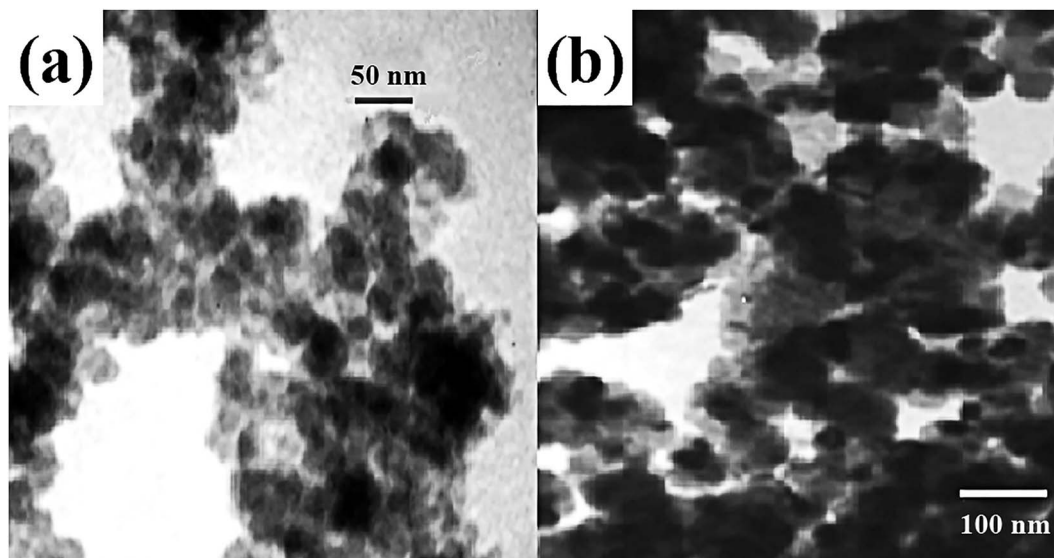


Fig. 6 TEM image of (a) MIONPs and (b) M-MIONPs.<sup>66</sup> This figure has been adapted from ref. 66 with permission from Elsevier.

$\text{Hg}(\text{OH})_2$ ,  $\text{HgClOH}$  and  $\text{HgCl}_2$ . It was reported that the  $\text{Hg}(\text{II})$  removal mechanisms were mainly surface complexation and flocculation–precipitation process, with the transformation from liquid phase to solid phase of  $\text{Hg}(\text{II})$ .  $40 \text{ mg L}^{-1}$  Mn–Fe oxide could effectively remove 80%  $\text{Hg}(\text{II})$  with the initial concentration of  $30 \text{ } \mu\text{g L}^{-1}$ , revealing a considerable adsorption efficiency and extensive low concentration limits for  $\text{Hg}(\text{II})$  solution. Besides, the Mn–Fe oxide required only 22 min to obtain the maximum  $\text{Hg}(\text{II})$  removal efficiency of 80%. This indicated the notable advantage of chemical adsorption through fast adsorption rate. The scheme for the formation mechanism of the Mn–Fe oxide and  $\text{Hg}(\text{II})$  removal mechanism, was depicted in Fig. 4. During the adsorption, the mercury species were removed as ligands, *via* surface complexation. The mercury preferred to form complexes with the active sites on the surface of the Mn–Fe oxide. The formed Hg–Mn–Fe complex flocculated into large particles, removing  $\text{Hg}(\text{II})$  *via* the transfer to the complex solid phase.

Except for inorganic metal oxides, organic macromolecule materials are also ideal chemical adsorbents for  $\text{Hg}(\text{II})$ . Some macromolecules can form well-organized organic functional group chains by self-assembly ways and these are combined with other active matters to make synergetic effects of adsorption.<sup>57–60</sup> Asif *et al.* synthesized a nuclear-shell hybrid material containing iron nanoparticles coated with chitosan and calixarene composite.<sup>61</sup> The organic calixarene macromolecules possess adsorptive activity. As Fig. 5 is shown, the calixarene molecule has abundant inner and outer functional groups, forming the size-adjustable cup-like cavity. Thus, the adsorbents can combine with  $\text{Hg}$  ions to form host-and-guest complex, obtaining the highest removal rate of  $\text{Hg}(\text{II})$  in all heavy metals. Zadmand *et al.* also fabricated calixarene-based crab-like molecular sensors for highly selective detection of mercury ions.<sup>62</sup> These similar organic macromolecules remove  $\text{Hg}(\text{II})$  through ligand exchange and complexation.

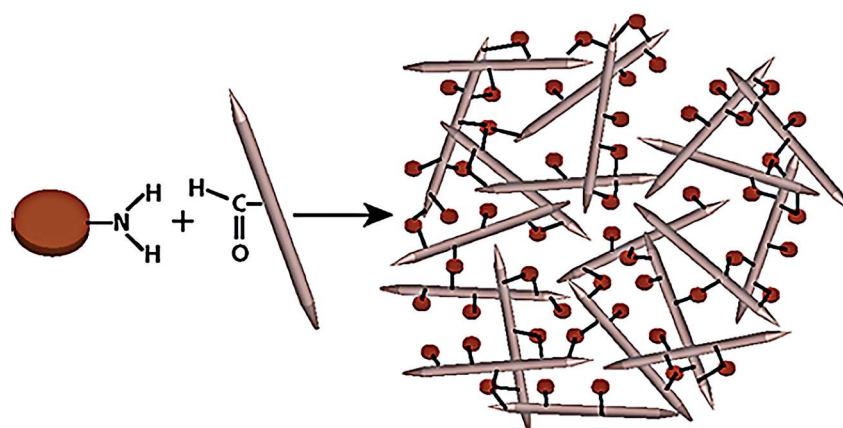


Fig. 7 Schematic of the preparation of the chemically crosslinked CNC/GQD hydrogel.<sup>95</sup> This figure has been adapted from ref. 95 with permission from ACS Nano.



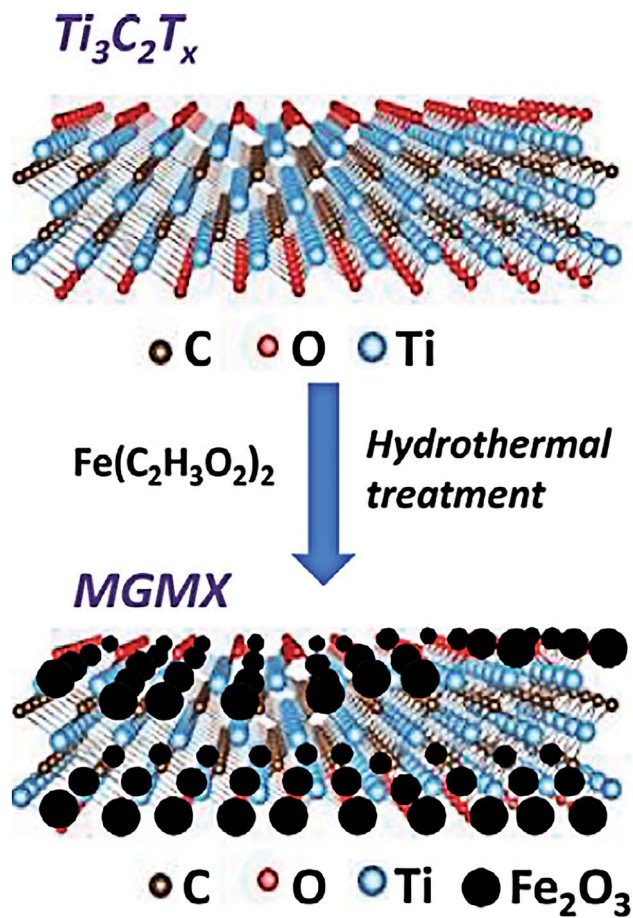


Fig. 8 Schematic structure of the composite formed by MXenes and  $\text{Fe}_2\text{O}_3$ .<sup>22</sup> This figure has been adapted from ref. 22 with permission from Elsevier.

Magnetic adsorbents are readily separated and recovered and can selectively remove the toxic pollutant from water.<sup>63</sup> Utilizing certain selective organic functional groups to modify the surface of magnetic adsorbent, the chemical adsorption performance would be further enhanced.<sup>64,65</sup> Parham *et al.* employed modified magnetic iron oxide with 2-mercapto-benzothiazole (MBT) to remove low-concentration of  $\text{Hg}(\text{II})$  from water effectively.<sup>66</sup> The adsorbent was easily prepared and achieved high removal efficiency within a very short time. The modified magnetic iron oxide nanoparticles (M-MIONPs) could adsorb up to 98.6% of  $50 \mu\text{g L}^{-1}$  of  $\text{Hg}(\text{II})$  and the complete removal process required just 4 min. Non-modified magnetic iron oxide nanoparticles (MIONPs) could remove only 43.47% for the same concentration of  $\text{Hg}(\text{II})$ . The obtained adsorption capacity of M-MIONPs for  $\text{Hg}(\text{II})$  was  $590 \mu\text{g g}^{-1}$ . The morphology of MIONPs was presented as aggregated flocs in the TEM image of Fig. 6. For M-MIONPs, MBT functional groups were coated on the surface of MIONPs. Such a fast adsorption with a superior removal efficiency was attributed to the strong affinity between the special organic functional ligand and  $\text{Hg}(\text{II})$ .<sup>67–70</sup> The outstanding adsorption performance of organic functional groups makes them promising compound for many other adsorbents. Mobina *et al.* also designed and grafted

aminopyrazole functional groups into multi-walled carbon nanotubes for the removal of  $\text{Hg}(\text{II})$ . The adsorption performance was remarkably enhanced.<sup>71</sup>

Other forms of chemical adsorbents, proteins or amino acid composite, and doped metal oxide composite, are also capable to display superior performance in heavy metal adsorption. Marcia *et al.* fabricated a novel mackinawite modified with L-cysteine as an active adsorbent for  $\text{Hg}(\text{II})$  removal.<sup>72</sup> Xu *et al.* added Sn and Fe into manganese oxide to obtain a novel  $\text{Fe-Sn-MnO}_x$  composite as an effective adsorbent for capturing mercury from coal-fired flue gas through chemical adsorption.<sup>73</sup> The adsorption performance of the composite was remarkably enhanced due to the synergetic effect of  $\text{Fe-Sn}$  and  $\text{MnO}_x$ . Compared to physical adsorption, chemical adsorption is faster and exhibits higher removal efficiency for  $\text{Hg}(\text{II})$ . This is because of the diversity of adsorption mechanism induced by abundant chemical functional groups.<sup>74–76</sup> However, chemical adsorption methods often suffer from secondary pollution of the adsorbents. The saturate adsorption capacity of chemical adsorption can still be promoted.<sup>77</sup>

### 2.3. Combination of physical adsorption and chemical adsorption for $\text{Hg}(\text{II})$ removal

For a preferable adsorption option, physical and chemical adsorptions can be combined to take the advantages of the both. Hence, these two adsorptions have been combined for porous structured materials with some modifications to attain higher adsorption performance. For example, hierarchical structure can be the basis of the combination of physical and chemical adsorption. Hierarchical morphology of an adsorbent is a significant impact factor on the adsorption performance.<sup>78</sup> Kim *et al.* fabricated hierarchically structured  $\text{MnO}_2$ -coated nanocomposite ( $\text{Fe}_3\text{O}_4/\text{MnO}_2$ ) for the efficient removal of  $\text{Hg}$  ions in aqueous.<sup>79</sup> The amorphous  $\text{MnO}_2$  coated on the composite has a flowerlike structure. The hierarchical structure has plenty of oxygen-containing groups on the surface of thin lamellae and a large BET surface area. The maximum adsorption capacity was up to  $53.2 \text{ mg g}^{-1}$ . Ravi *et al.* also fabricated novel hierarchically dispersed mesoporous silica spheres as effective adsorbents, whose hierarchically mesoporous structure ensured superior thermodynamic behaviors in the adsorption process.<sup>80</sup> Fardmousavi *et al.* synthesized a thiol-functionalized hierarchical zeolite nanocomposite for  $\text{Hg}(\text{II})$  adsorption.<sup>81</sup> The zeolite nanocomposite combines the strongly hydrothermal stability of zeolites with the superior mass transport property of mesoporous materials. Thus, this adsorbent displayed excellent ability to bind  $\text{Hg}(\text{II})$  with a high selectivity and achieved an adsorption capacity of  $8.2 \text{ mequiv. g}^{-1}$ . From the microcosmic perspective, the 3D hierarchically structure consists of mainly micropores and mesopores. The micropores directly lead to the enhanced adsorption capacity. Meanwhile, the well-developed mesopores promoted the optimum adsorption kinetics.<sup>82</sup> The mesopores channels serve as liquid flow pathways and allow for the fast transport of  $\text{Hg}(\text{II})$  to the active adsorption sites.





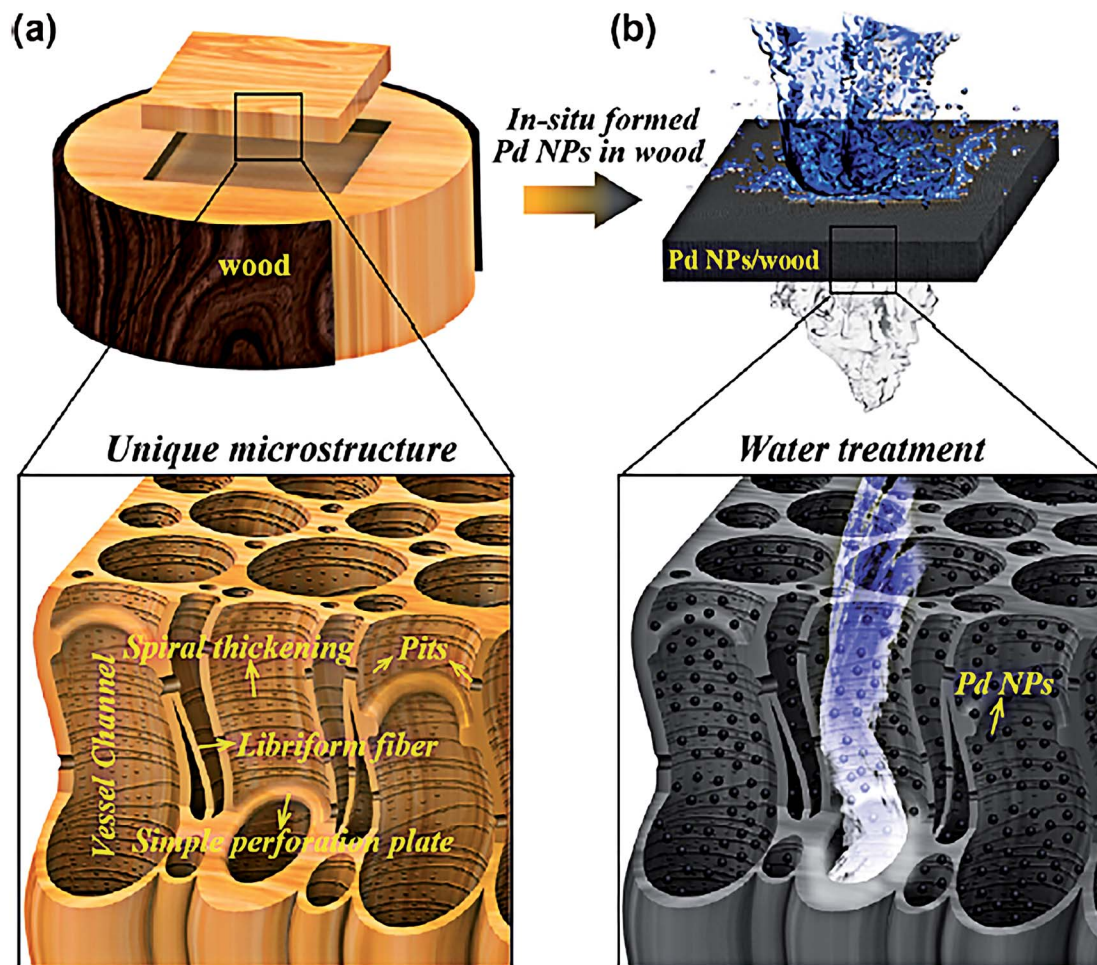


Fig. 9 (a) Schematic of a 3D wood membrane decorated with Pd NPs for water treatment. (b) *In situ* formed Pd NPs (black dots) within the wood demonstrated the plasmonic effect inside the wood channels.<sup>107</sup> This figure has been adapted from ref. 107 with permission from ACS Nano.

On the other hand, surface interaction is the core of combination of physical and chemical adsorption. Faulconer *et al.* impregnated the activated carbon with iron oxide to fabricate a composite MPAC (magnetic powdered activated carbon) which achieved a high Hg(II) removal efficiency of 96.3% with a sorbent recovery ratio of 92.5%.<sup>83</sup> The recovery of the adsorbent was achieved by magnetic separation. This composite adsorbent could remove Hg(II) to obtain the final concentration of  $0.2 \mu\text{g L}^{-1}$ . The high performance was attributed to iron oxide that in the adsorption process formed strong binding affinity with Hg species and offered many adsorption sites for Hg(II) through coordination with oxygen atoms. Yao Li

*et al.* also fabricated N-doped porous carbon with magnetic particles ( $\text{Fe}_3\text{O}_4$  and Fe) formed *in situ* for heavy metal removal.<sup>84</sup> The high adsorption capacity ( $16 \text{ mg g}^{-1}$ ) was resulted by the synergetic effects of physical adsorption from the surface area and chemical adsorption from complexation interaction. Na Yang *et al.* also synthesized magnetic activated carbon nanocomposite modified by  $\text{Fe}_3\text{O}_4$  particles applied for water purification, contributed from combination of physical adsorption and chemical adsorption.<sup>85</sup>

Physical adsorption itself provided by porous materials with large surface areas is insufficient for Hg(II) removal. Contrary to this, chemical adsorption brings strong synergetic effects

Table 3 Comparison of various adsorbents with physical adsorption

No.	Adsorbent	BET surface area	Hg(II) removal efficiency	Adsorption capacity	Ref.
1	Activated carbon	$1690 \text{ m}^2 \text{ g}^{-1}$	~82%	$0.869 \text{ mg g}^{-1}$	26
2	Porous carbon	$780 \text{ m}^2 \text{ g}^{-1}$	~95%	$151.5 \text{ mg g}^{-1}$	27
3	Activated carbon	$555 \text{ m}^2 \text{ g}^{-1}$	60–80%	$128 \text{ mg g}^{-1}$	28
4	ZSM-5 zeolite	$189 \text{ m}^2 \text{ g}^{-1}$	96.3%	$51.54 \text{ mg g}^{-1}$	29
5	ACF	$848\text{--}1259 \text{ m}^2 \text{ g}^{-1}$	—	$290\text{--}710 \text{ mg g}^{-1}$	41





Table 4 Comparison of various adsorbents with chemical adsorption (BET surface area is irrelevant)

No.	Adsorbent	BET surface area	Hg(II) removal efficiency	Adsorption capacity	Ref.
1	Ag-Zn nanoparticles	—	92%	554 mg g <sup>-1</sup>	55
2	Mn-Fe oxides	—	80%	—	56
3	Calixarene/Fe hybrid	—	~90%	0.43 μM g <sup>-1</sup>	61
4	Modified Fe oxide	—	98.6%	0.59 mg g <sup>-1</sup>	66
5	Fe-Sn-MnO <sub>x</sub>	—	—	3.75 mg g <sup>-1</sup>	73

through effective interaction such as oxidation–reduction reaction.<sup>86</sup> Moghaddam *et al.* prepared MnO<sub>2</sub>-coated carbon nanotubes (MnO<sub>2</sub>/CNT) to remove Hg(II) from aqueous solution and obtained 58.8 mg g<sup>-1</sup> adsorption capacity, in which MnO<sub>2</sub> went through oxidation–reduction reactions.<sup>87</sup> Manganese oxides have superior chemical adsorption properties with Hg(II). The highly conjugated CNT walls provided (i) Hg(II) ions with both van der Waals and electrostatic interactions and (ii) the adsorbent matrix with electrical conductivity for surface charge transport. Moreover, the high-conductive CNT was negatively charged after an acidic treatment, the CNT will improve the adsorption performance of the composite on Hg(II) ions. Furthermore, Xu *et al.* synthesized 3D MnO<sub>2</sub>/carbon sphere composite for the catalytic oxidation and adsorption of Hg.<sup>88</sup> Carbon spheres served as the core and MnO<sub>2</sub> nanorods grew on the surface of carbon spheres, leading to the enlargement of surface areas and pore volumes. The final removal efficiency was up to 99%, benefiting from the chemical oxidation and physical adsorption.

Besides active metal oxides, many chemical compounds can be combined with porous matrix materials to achieve the synergetic effects of physical and chemical adsorptions as adsorbent. For instance, the combination of porous carbon and polymer brings not only large surface area from the pore structure but also masses of functional groups from the synthesis of polymer. Moonjung *et al.* synthesized polypyrrole-impregnated porous carbon *via* vapor infiltration polymerization.<sup>89</sup> Owing to the amine groups of polypyrrole, the modified porous carbon revealed superior binding affinity for metal ions like Hg(II). The adsorption efficiency of this modified porous carbon was 20 times higher than that of other similar adsorbent with amine groups. In addition, carbon nanotubes (CNT) can

also be organically modified to enhance the adsorption performance. Hadavifar *et al.* introduced amine and thiol functional groups onto the walls of CNT to obtain the functionalization of multi-walled CNT.<sup>90</sup> Due to the synergetic effects of CNT and organic groups, the adsorbent could achieve the Hg(II) removal capacity of 105.65 mg g<sup>-1</sup> and removal efficiency of 88.7%. Saleh *et al.* also fabricated silica and CNT composite (SiO<sub>2</sub>-CNT) for Hg(II) removal and the removal efficiency reached up to above 98% after five adsorption circles.<sup>91</sup>

As a 1D material, crystal nanocellulose (CNC) fabricated from plants is also promising material for Hg(II) removal, for its cross-linking structure and large surface area.<sup>92–94</sup> Moien *et al.* fabricated a nanocolloidal hydrogel formed by CNC and graphene quantum dots (GQD).<sup>95</sup> As shown in Fig. 7, the CNC and GQD were combined through the surface organic functional groups by chemical cross-linking reaction, utilizing the advantage of molecular hydrogels and nanoparticle-based scavengers. By selecting different ratio of CNC to GQD, the structure of the composite can be adjusted from lamellar to nanofiber, with the change of hydrogel permeability. The scavenging capacity for Hg(II) can be obtained up to 164 mg g<sup>-1</sup> after first adsorption circle and 120 mg g<sup>-1</sup> after second circle. The nanocolloidal hydrogel exhibited outstanding adsorption capacity and good recyclability, attributed to the large surface area of nanohydrogel and abundance of ion-coordinating sites on the surface of nanoparticle quantum dots. In other studies, cellulose was also modified with guanlyl groups and used for heavy metal removal.<sup>96</sup> The participation of active functional groups led to the wide-range adsorption performance on Hg(II) and many other heavy metal ions. CNC can also form membrane but its mechanical properties still require improvement.<sup>97,98</sup>

Table 5 Comparison of various adsorbents involving both physical and chemical adsorption

No.	Adsorbent	BET surface area	Hg(II) removal efficiency	Adsorption capacity	Ref.
1	Thiol-functionalized zeolite	82 m <sup>2</sup> g <sup>-1</sup>	—	8.2 mequiv. g <sup>-1</sup>	81
2	MPAC	790.11 m <sup>2</sup> g <sup>-1</sup>	96.3%	—	83
3	Polyamide magnetic palygorskite	380 m <sup>2</sup> g <sup>-1</sup>	95%	211 mg g <sup>-1</sup>	86
4	MnO <sub>2</sub> /CNT	110.38 m <sup>2</sup> g <sup>-1</sup>	91.7%	58.8 mg g <sup>-1</sup>	87
5	MnO <sub>2</sub> /carbon sphere	134.1 m <sup>2</sup> g <sup>-1</sup>	99%	—	88
6	MWCNTs-SH	—	88.7%	105.65 mg g <sup>-1</sup>	90
7	SiO <sub>2</sub> /CNT	—	98%	140 mg g <sup>-1</sup>	91
8	Nanocolloidal hydrogel (CNC/GQD)	~500 m <sup>2</sup> g <sup>-1</sup>	—	164 mg g <sup>-1</sup>	95
9	Ti <sub>3</sub> C <sub>2</sub> T <sub>x</sub> /Fe <sub>2</sub> O <sub>3</sub>	56.51 m <sup>2</sup> g <sup>-1</sup>	99.9%	1128.41 mg g <sup>-1</sup>	22
10	GO/Fe-Mn	153 m <sup>2</sup> g <sup>-1</sup>	91.1%	43.88 mg g <sup>-1</sup>	113



With the development of advanced materials, novel two-dimensional (2D) nanosheets or membranes materials (MXenes, boron nitride, graphene oxide and conjugated polymers *etc.*) have recently attracted much attention for remediation and treatment for water.<sup>99–101</sup> Meanwhile, the functionalization and surface modification of 2D material adsorbents improve the metal ion trapped capacity and comprehensive adsorption performance. 2D MXenes are one of the most popular structure materials investigated in recent years.<sup>102</sup> Liu *et al.* studied an ultrathin 2D MXene membrane and its outstanding performance in nanofiltration.<sup>103</sup> Shahzad *et al.* developed a recoverable titanium carbide magnetic nanocomposite to capture Hg(II) ions in wastewater, as shown in Fig. 8.<sup>22</sup> The hybrid nanocomposite was formed from Ti<sub>3</sub>C<sub>2</sub>T<sub>x</sub> MXene and Fe<sub>2</sub>O<sub>3</sub> nanoparticles using a facile hydrothermal method. The 2D hybrid composite finally demonstrated a maximum experimental Hg(II) uptake capacity of 1128.41 mg g<sup>-1</sup>, and could adsorb ~99.9% Hg(II) in the presence of background metal ions. After the adsorption and desorption tests, the composite showed excellent recyclability of up to five adsorption/desorption circles. The graphene-like 2D nanolayer structure of titanium carbides provided a high surface area for physical adsorption. Meanwhile, the ferric oxide nanoparticles offered plenty of coordinate sites for chemical adsorption. Among numerous 2D materials, boron nitride (BN) based materials also have potential application in environment remediation. BN nanosheets with a structure like graphene possess large surface area and high chemical stability. BN-based composite materials could removal heavy metals in water mainly through the mechanisms of surface complexation,  $\pi$ - $\pi$  stacking and electrostatic interactions.<sup>104</sup> The synergetic effect of physical and chemical adsorptions brought supreme performance for Hg(II) removal.

Membrane materials show great potential in water purification, owing to their high degrees of mechanical strength and excellent reusability.<sup>105,106</sup> Wood is ubiquitously used as a raw structural material for Hg(II) removal. Chen *et al.* fabricated mesoporous 3D wood membrane decorated with Pd nanoparticles for highly efficient water treatment.<sup>107</sup> This kind of wood membrane material was original and didn't require complicated process of calcination. As Fig. 9 is shown, natural wood contained partially aligned nanochannels and lumens that stretch along its growth direction, which afforded plenty of active sites for physical adsorption. Additionally, Pd nanoparticles showed excellent catalytic properties thus could promote chemical adsorption on Hg(II). The wood membrane composites exhibited high removal efficiency of 99.8% at a treatment flow rate up to  $1 \times 10^5$  L m<sup>-2</sup> h<sup>-1</sup>. Song *et al.* also prepared a nature-inspired flexible 3D porous wood membrane *via* a facile one-step chemical treatment method directly from natural wood.<sup>108</sup> The superb flexibility and facile modification on the wood membrane made it efficient material for water treatment. Moreover, wood membrane is more advantageous than powder adsorbents owing to the high flux rate of the abundant open vessel channels, as well as natural abundance and biodegradability.<sup>109</sup> Except for wood membrane, some other flexible and modifiable membranes such as carbon paper films,

polyacrylonitrile or cellulose membranes are also promising candidates for Hg(II) removal. These materials are not only ultrathin but also possess stable chemical resistance, high recycling performance and excellent antifouling properties.<sup>110–112</sup>

### 3. Remarks on the different adsorption methods

The Hg(II) removal capacities and efficiencies of some typical adsorbents reported in the literatures above are summarized in the tables below. Generally, porous carbon, activated carbon fibers and zeolites as adsorbents work through physical adsorptions. While, metal oxides, organic macromolecules and functionally modified metal oxides work through chemical adsorptions; carbon-based composites (MPAC), functionalized CNC, 2D MXenes, boron nitride, polymer composites and the rest mainly involve both physical and chemical adsorptions.

From Table 3, it is evident that the adsorbents with physical adsorption usually possess high BET surface area. Porous structured carbon materials and zeolites exhibit relatively high Hg(II) removal efficiency. Activated carbon fiber has excellent adsorption capacity. The improvement of removal efficiency and adsorption capacity still attracts further investigation by researchers. Table 4 indicates that the adsorbents with chemical adsorption play their role through chemical interactions rather than surface area. The metal oxides combined with active organic functional groups have the highest removal efficiency. However, the adsorption capacity of these adsorbents requires further improvement.

As Table 5 is shown, most adsorbents which involve both physical and chemical adsorption possess high Hg(II) removal efficiency and outstanding adsorption capacity, respectively. On one hand, the hierarchically structured matrix of these composites with large surface area plays its role in physical adsorption, typically as MPAC and polyamide magnetic palygorskite. On the other hand, active oxides and organic compounds make contribution in chemical adsorption. In particular, materials like MnO<sub>2</sub>/carbon sphere and SiO<sub>2</sub>/CNT reveal splendid removal efficiency for Hg(II). It is noteworthy that new emerging titanium carbide materials have the extremely high adsorption capacity and supreme adsorption efficiency. The fact may open a new avenue for the exploration of novel 2D advanced materials in the field of water treatment.

For these types of materials, the mechanisms of physical adsorption mainly include van der Waals interaction and electrostatic attraction to benefit from the high surface area of porous material adsorbents. The mechanisms of chemical adsorption often involve ligand exchange, surface complexation and oxidation–reduction reaction, sometimes along with flocculation–precipitation process. Generally, physical adsorption is multilayer adsorption, but chemical adsorption is monolayer due to its space limitation. Commonly, pseudo-first order model and pseudo-second order model are used to simulate the kinetics data of adsorption. Pseudo-first order model indicates the adsorption process is up by diffusion of adsorbents while pseudo-second order model highlights the interaction of matters. Furthermore, the adsorption isotherms models mainly



include the Langmuir isotherm model and the Freundlich isotherm model. The Langmuir isotherm model corresponds to monolayer adsorption with all binding sites equal, which is often consistent with pure chemical adsorption. The Freundlich isotherm model describes multilayer adsorption with adsorption energy different on a heterogeneous surface, which is always related with combination of physical adsorption and chemical adsorption.

From our perspectives, the following criteria are proposed for the development of ideal adsorbents for Hg(II) removal:

- Hierarchical porous structure offers aqueous accessible tunnel networks and mesopores channels as liquid flow pathways and allows for the fast transport of Hg(II) to the active adsorption sites,

- The combination of physical adsorption benefited from large surface areas and chemical adsorption provided from large numbers of functional group binding sites brings potential synergetic effects,

Thus, a composite that consists of a hierarchically structured porous matrix with a high surface area and adsorptive-active nanoparticles which are dispersed in the porous matrix, should have an excellent performance in terms of the removal of Hg(II).

## 4. Conclusion

In summary, we discussed the principles of Hg(II) adsorption and clarified the relationships between the structure and performance of adsorbents by reviewing research progress in recent decades on physical adsorption and chemical adsorption. The combination of physical adsorption and chemical adsorption exhibits a superior performance than physical or chemical adsorption alone. The main advantages of physical adsorption are low cost and simple operation process. Chemical adsorption, on the other hand, brings fast adsorption rate and high adsorption capacity. The combination of the both has been of great interests due to the synergetic effects of the large surface area and functional complexation interaction. This review provides a comprehensive view on the design of an efficient composite adsorbent and explores the potentials of nanocomposite materials for Hg(II) and other heavy metal treatment with high performance. There are still many challenges in the development of adsorbents for Hg(II) removal. The regeneration performance of the adsorbents still deserves our study to improve and the adsorbed heavy metal ions need to be recovered and reused. Also, the adsorption capacity of the adsorbents can be well improved with the more and more advanced nanomaterial technology.

## Conflicts of interest

There are no conflicts to declare.

## Acknowledgements

The authors gratefully acknowledge the financial support from National Key R&D Program of China (2016YFA0202900, 2016YFC1402400), NSFC (51672173), Shanghai Science and Technology committee (17JC1400700, 18520744700), Science

and Technology Planning Project of Guangdong Province (2016A010103018).

## References

- 1 M. Yeganeh, M. Afyuni, A.-H. Khoshgoftarmanesh, L. Khodakarami, M. Amini, A.-R. Soffyanian and R. Schulin, *J. Hazard. Mater.*, 2013, **244–245**, 225–239.
- 2 USEPA, *Mercury Study Report to Congress*, EPA-452/R-97-005, 1997.
- 3 P. Miretzky and A. F. Cirelli, *J. Hazard. Mater.*, 2009, **167**, 10–23.
- 4 W. B. Lyons, D. M. Wayne, J. J. Warwick and G. A. Doyle, *Environ. Geol.*, 1998, **34**, 143–150.
- 5 R. P. Mason, J. R. Reinfelder and F. M. M. Morel, *Environ. Sci. Technol.*, 1996, **30**, 1835–1845.
- 6 Z. Chen, Z. Geng, Z. Zhang, L. Ren, T. Tao, R. Yang and Z. Guo, *Eur. J. Inorg. Chem.*, 2014, **2014**, 3172–3177.
- 7 D. Fox and A. Sillman, *Science*, 1979, **206**, 78–80.
- 8 M. Y. Ren, S. M. Ding, Z. Fu, L. Y. Yang, W. Y. Tang, D. C. W. Tsang, D. Wang and Y. Wang, *J. Hazard. Mater.*, 2019, **367**, 427–436.
- 9 Q. Tang, A. L. Collins, A. B. Wen, X. B. He, Y. H. Bao, D. C. Yan, Y. Long and Y. S. Zhang, *Sci. Total Environ.*, 2018, **633**, 1114–1125.
- 10 Y. K. Wang, N. Zhang, D. Wang, J. C. Wu and X. Zhang, *Sci. Total Environ.*, 2018, **624**, 1187–1194.
- 11 M. M. Matlock, B. S. Howerton and D. A. Atwood, *J. Hazard. Mater.*, 2001, **84**, 73–82.
- 12 S. Chiarle, M. Ratto and M. Rovatti, *Water Res.*, 2000, **34**, 2971–2978.
- 13 D. Sevdic, L. Fekete and H. Meider, *J. Inorg. Nucl. Chem.*, 1980, **42**, 885–889.
- 14 D. S. Han, M. Orillano, A. Khodary, Y. Duan, B. Batchelor and A. Abdel-Wahab, *Water Res.*, 2014, **53**, 310–321.
- 15 V. Antochshuk and M. Jaroniec, *Chem. Commun.*, 2002, **3**, 258.
- 16 H. Xu, J. Xie, Y. Ma, Z. Qu, S. Zhao, W. Chen, W. Huang and N. Yan, *Fuel*, 2015, **140**, 803–809.
- 17 R. Yu, Y. Shi, D. Yang and Z.-Z. Yu, *ACS Appl. Mater. Interfaces*, 2017, **9**, 21809–21819.
- 18 N. Chitpong and S. M. J. Husson, *J. Membr. Sci.*, 2017, **523**, 418–429.
- 19 J. Tang, H. Lv, Y. Gong and Y. Huang, *Bioresour. Technol.*, 2015, **196**, 355–363.
- 20 P. Bonnissel-Gissinger, M. Alnot, J.-P. Lickes, J.-J. Ehrhardt and P. Behra, *J. Colloid Interface Sci.*, 1999, **215**, 313–322.
- 21 C. Fischer, M. Oschatz, W. Nickel, D. Leistenschneider, S. Kaskel and E. Brunner, *Chem. Commun.*, 2017, **53**, 4845–4848.
- 22 A. Shahzad, K. Rasool, W. Miran, M. Nawaz, J. Jang, K. A. Mahmoud and D. S. Lee, *J. Hazard. Mater.*, 2018, **344**, 811–818.
- 23 S.-H. Park, S. O. Hwang, T.-S. Kim, A. Cho, S. J. Kwon, K. T. Kim, H.-D. Park and J.-H. Lee, *Appl. Surf. Sci.*, 2018, **443**, 458.





- 24 K. Kadirvelu, M. Kavipriya, C. Karthika, M. Radhika, N. Vennilamani and S. Pattabhi, *Bioresour. Technol.*, 2003, **87**, 129–132.
- 25 H. Fornwalt and R. Hutchins, *Chem. Eng. J.*, 1966, **73**, 179.
- 26 G. Skodras, I. Diamantopoulou, A. Zabaniotou, G. Stavropoulos and G. P. Sakellariopoulos, *Fuel Process. Technol.*, 2007, **88**, 749–758.
- 27 M. Zabihi, A. Haghighi Asl and A. Ahmadpour, *J. Hazard. Mater.*, 2010, **174**, 251–256.
- 28 F.-S. Zhang, J. O. Nriagu and H. Itoh, *Water Res.*, 2005, **39**, 389–395.
- 29 S. Rostami, S. N. Azizi and N. Asemi, *J. Iran. Chem. Soc.*, 2018, **15**(8), 1741–1754.
- 30 M. S. Holm, E. Taarning, K. Egeblad and C. H. Christensen, *Catal. Today*, 2011, **168**, 3–16.
- 31 J. Zheng, X. Zhang, Y. Zhang, J. Ma and R. Li, *Microporous Mesoporous Mater.*, 2009, **122**, 264.
- 32 J. Liu and X. Du, *J. Mater. Chem.*, 2011, **21**, 6981.
- 33 D. He, X. He, K. Wang, Y. Zhao and Z. Zou, *Langmuir*, 2013, **29**, 5896.
- 34 M. Yin, Z. Li, Z. Liu, N. Yang and J. Ren, *ACS Appl. Mater. Interfaces*, 2012, **4**, 431.
- 35 M. Jamshidi Shadbad, A. Mohebbi and A. Soltani, *Korean J. Chem. Eng.*, 2011, **28**, 1029.
- 36 S. N. Azizi, A. Roozbehani Dehnavi and A. Joorabdoozh, *Mater. Res. Bull.*, 2013, **48**, 1753.
- 37 Y. Li, M. Xia and S. Zhu, *J. Hazard. Mater.*, 2019, **371**, 33–41.
- 38 K. G. Bhattacharyya and S. Sen Gupta, *Ind. Eng. Chem. Res.*, 2006, **45**(21), 7232–7240.
- 39 K. G. Bhattacharyya and S. Sen Gupta, *Ind. Eng. Chem. Res.*, 2006, **45**, 7232–7240.
- 40 Z. M. Lei, Q. D. An, Y. Fan, J. L. Lv, C. Gao, S. R. Zhai and Z. Y. Xiao, *New J. Chem.*, 2015, **40**, 1195–1204.
- 41 J. V. Nabais, P. J. M. Carrott, M. M. L. R. Carrott, M. Belchior, D. Boavida, T. Dially and I. Gulyurtlu, *Appl. Surf. Sci.*, 2006, **252**, 6046–6052.
- 42 C. Thamaraiselvan, S. Lerman, K. Weinfeld-Cohen and C. G. Dosoretz, *Sep. Purif. Technol.*, 2018, **202**, 1–8.
- 43 S. Jeon, C. H. Park, S.-H. Park, M. G. Shin, H.-J. Kim, K.-Y. Baek, E. P. Chan, J. Bang and J.-H. Lee, *J. Membr. Sci.*, 2018, **555**, 369.
- 44 A. Malekizadeh and P. M. Schenk, *Sci. Rep.*, 2017, **7**(1), 17437.
- 45 S. Shultz, M. Bass, R. Semiat and V. Freger, *J. Membr. Sci.*, 2018, **546**, 165.
- 46 F. Asempour, D. Emadzadeh, T. Matsuura and B. Kruczek, *Desalination*, 2018, **439**, 179.
- 47 A. Pereira, A. Martins, A. Paulino, A. Fajardo, M. Guilherme, M. Faria, G. Linde, A. Rubira and E. Muniz, *Rev. Virtual Quim.*, 2017, **9**, 1.
- 48 M. Guilherme, F. Aouada and E. Muniz, *Eur. Poly. J.*, 2015, **72**, 365.
- 49 D. Staneva, T. Koutzarova, B. Vertruyen, E. Vasileva-Tonkova and I. Grabchev, *J. Mol. Struct.*, 2017, **1127**, 74–80.
- 50 M. K. Uddin, *Chem. Eng. J.*, 2017, **308**, 438–462.
- 51 M. Alimohammady and M. Jahangiri, *J. Appl. Chem.*, 2017, **11**, 75.
- 52 M. Ma, R. Liu, H. Liu and J. Qu, *Water Res.*, 2012, **46**, 73–81.
- 53 I. Samanta and S. Bandyopadhyay, *Pet bird diseases and care*, Springer, 2017, vol. 6, pp. 253–262.
- 54 L. Jiang, S. Xiao and J. Chen, *Colloids Surf., A*, 2015, **479**, 1–10.
- 55 A. Ali, A. Mannanb, I. Hussainc, I. Hussaind and M. Zia, *Environmental Nanotechnology, Monitoring and Management*, 2018, **9**, 1–11.
- 56 X. Lu, X. Huangfu and J. Ma, *J. Hazard. Mater.*, 2014, **280**, 71–78.
- 57 L. Lin and C. Zou, *J. Chem. Eng. Data*, 2017, **62**, 762–772.
- 58 C. Leostean, O. Pana, M. Stefan, A. Popa, D. Toloman, M. Senila, S. Gutoiu and S. Macavei, *Appl. Surf. Sci.*, 2018, **427**, 192–201.
- 59 A. Azari, H. Gharibi, B. Kakavandi, G. Ghanizadeh, A. Javid, A. H. Mahvi, K. Sharafi and T. Khosravia, *J. Chem. Technol. Biotechnol.*, 2017, **92**, 188–200.
- 60 S. Loganathan, R. B. Valapa, R. K. Mishra, G. Pugazhenthii and S. Thomas, *Thermal and Rheological Measurement Techniques for Nanomaterials Characterization*, Elsevier, 2017, vol. 1, pp. 67–108.
- 61 A. Bhattia, M. Oguza and M. Yilmaz, *Appl. Surf. Sci.*, 2018, **434**, 1217–1223.
- 62 R. Zadward, P. Akbari-Moghaddam and S. Darvishi, *Supramol. Chem.*, 2017, **29**, 17–23.
- 63 P. Thanabalasingam and W. F. Pickering, *Environ. Pollut.*, 1985, **10**, 115–128.
- 64 R. A. Lockwood and K. Y. Chen, *Environ. Sci. Technol.*, 1973, **7**, 1028–1034.
- 65 G. I. Danmaliki, T. A. Saleh and A. A. Shamsuddeen, *Chem. Eng. J.*, 2017, **313**, 993.
- 66 H. Parham, B. Zargar and R. Shiralipour, *J. Hazard. Mater.*, 2012, **205**, 94–100.
- 67 C. Chen and Y.-J. Chen, *Tetrahedron Lett.*, 2004, **45**, 113–115.
- 68 X.-J. Mu, J.-P. Zou, R.-S. Zeng and J.-C. Wu, *Tetrahedron Lett.*, 2005, **46**, 4345–4347.
- 69 M. Mazloum, M. K. Amini and I. Mohammadpoor-Baltork, *Sens. Actuators, B*, 2000, **63**, 80–85.
- 70 J. Chwastowska, A. Rogowska, E. Sterlińska and J. Dudek, *Talanta*, 1999, **49**, 837–842.
- 71 M. Alimohammady, M. Jahangiri, F. Kiani and H. Tahermansouri, *Res. Chem. Intermed.*, 2018, **44**, 69–92.
- 72 M. R. M. Chaves, K. T. Valsaraj, R. P. Gambrell and R. Delaune, *Environmental Research Science & Technology*, 2017, **1**(1), 16–29.
- 73 H. Xu, J. Xie, Y. Ma, Z. Qu, S. Zhao, W. Chen, W. Huang and N. Yan, *Fuel*, 2015, **140**, 803–809.
- 74 M. Alimohammady, M. Jahangiri, F. Kiani and H. Tahermansouri, *J. Environ. Chem. Eng.*, 2017, **5**, 3405.
- 75 S. O. Adio, M. H. Omar, M. Asif and T. A. Saleh, *Process Saf. Environ.*, 2017, **107**, 518.
- 76 T. A. Saleh, A. Sari and M. Tuzen, *J. Environ. Chem. Eng.*, 2017, **5**, 1079.
- 77 H. Dong, Z. Jiang, J. Deng, C. Zhang, Y. Cheng, K. Hou, L. Zhang, L. Tang and G. Zeng, *Water Res.*, 2018, **129**, 51–57.



- 78 H. Mao and Z. Liu, *Spectrochim. Acta, Part A*, 2018, **189**, 366–373.
- 79 E.-J. Kim, C.-S. Lee, Y.-Y. Chang and Y.-S. Chang, *ACS Appl. Mater. Interfaces*, 2013, **5**, 9628–9634.
- 80 S. Ravi, M. Selvaraj, H. Park, H.-H. Chun and C.-S. Ha, *New J. Chem.*, 2014, **38**, 3899–3906.
- 81 O. Fardmousavi and H. Faghian, *C. R. Chim.*, 2014, **17**, 1203–1211.
- 82 M. Rose, Y. Korenblit, E. Kockrick, L. Borchardt, M. Oschatz, S. Kaskel and G. Yushin, *Small*, 2011, **7**, 1108–1117.
- 83 E. K. Faulconer, N. V. von Reitzenstein and D. W. Mazyck, *J. Hazard. Mater.*, 2012, **199–200**, 9–14.
- 84 Y. Li, S. Zhu, Q. Liu, Z. Chen, J. Gu, C. Zhu, T. Lu, D. Zhang and J. Ma, *Water Res.*, 2013, **47**, 4188–4197.
- 85 N. Yang, S. Zhu, D. Zhang and S. Xu, *Mater. Lett.*, 2008, **62**, 645–647.
- 86 T. Saleh, M. Tuzen and A. Sari, *J. Environ. Manage.*, 2018, **211**, 323–333.
- 87 H. K. Moghaddam and M. Pakizeh, *J. Ind. Eng. Chem.*, 2015, **21**, 221–229.
- 88 H. Xu, J. Jia, Y. Guo, Z. Qu, Y. Liao, J. Xie, W. Shangguan and N. Yan, *J. Hazard. Mater.*, 2018, **342**, 69–76.
- 89 M. Choi and J. Jang, *J. Colloid Interface Sci.*, 2008, **325**, 287–289.
- 90 M. Hadavifar, N. Bahramifar, H. Younesi and Q. Li, *Chem. Eng. J.*, 2014, **237**, 217–228.
- 91 T. A. Saleh, *Environ. Sci. Pollut. Res.*, 2015, **22**, 16721–16731.
- 92 K. Bethke, S. Palantöken, V. Andrei, M. Roß, V. Raghuwanshi, F. Kettemann, K. Greis, T. Ingber, J. Stückrath, S. Valiyaveetil and K. Rademann, *Adv. Funct. Mater.*, 2018, **28**, 1800409.
- 93 A. B. Seabra, J. S. Bernardes, W. J. Fávaro, A. J. Paula and N. Durán, *Carbohydr. Polym.*, 2018, **181**, 514.
- 94 H. Farid, A. Saeidi, M. Farzaneh and F. Erchiqui, *Cold Reg. Sci. Technol.*, 2018, **146**, 81.
- 95 M. Alizadehgiashi, N. Khuu, A. Khabibullin, A. Henry, M. Tebbe, T. Suzuki and E. Kumacheva, *ACS Nano*, 2018, **9**, 1148–1151.
- 96 I. M. Kenawy, M. A. H. Hafez, M. A. Ismail and M. A. Hashem, *Int. J. Biol. Macromol.*, 2018, **107**, 1538–1549.
- 97 C. Park, S. Jeon, S. Park, M. Shin, M. Park, S. Leec and J. Lee, *J. Mater. Chem. A*, 2019, **7**, 3992.
- 98 J. Lv, G. Zhang, H. Zhang and F. Yang, *Chem. Eng. J.*, 2018, **352**, 765–773.
- 99 C. Tan, X. Cao, X. J. Wu, Q. He, J. Yang, X. Zhang, J. Chen, W. Zhao, S. Han, G. H. Nam, M. Sindoro and H. Zhang, *Chem. Rev.*, 2017, **117**(9), 6225–6331.
- 100 T. Liu, B. Yang, N. Graham, W. Yu and K. Sun, *J. Membr. Sci.*, 2017, **542**, 31–40.
- 101 N. Zhang, T. Wang, X. Wu, C. Jiang, T. Zhang, B. Jin, H. Ji, W. Bai and R. Bai, *ACS Nano*, 2017, **11**(7), 7223–7229.
- 102 S. Torrellasab, M. Munoz, J. Gläselc, Z. Pedroa, C. Domínguezb, J. Garcíaab, B. Etzoldc and J. A. Casas, *Chem. Eng. J.*, 2018, **347**, 595–606.
- 103 G. Liu, J. Shen, Q. Liu, G. Liu, J. Xiong, J. Yang and W. Jin, *J. Membr. Sci.*, 2018, **548**, 548–558.
- 104 S. Yu, X. Wang, H. Pang, R. Zhang, W. Song, D. Fu, T. Hayat and X. Wang, *Chem. Eng. J.*, 2018, **333**, 343–360.
- 105 W. Liu, M. Song, B. Kong and Y. Cui, *Adv. Mater.*, 2017, **29**, 1603436.
- 106 L. Zhou, S. Zhuang, C. He, Y. Tan, Z. Wang and J. Zhu, *Nano Energy*, 2017, **32**, 195–200.
- 107 F. Chen, A. Gong, M. Zhu, G. Chen, S. Lacey, F. Jiang, Y. Li, Y. Wang, J. Dai, Y. Yao, J. Song, B. Liu, K. Fu and L. Hu, *ACS Nano*, 2017, **11**, 4275–4282.
- 108 J. Song, C. Chen, C. Wang, Y. Kuang, Y. Li, F. Jiang, Y. Li, E. Hitz, Y. Zhang, B. Liu, A. Gong, H. Bian, J. Y. Zhu, J. Zhang, J. Li and L. Hu, *ACS Appl. Mater. Interfaces*, 2017, **9**, 23520–23527.
- 109 J. Lv, G. Zhang, H. Zhang, C. Zhao and F. Yang, *Appl. Surf. Sci.*, 2018, **440**, 1091–1100.
- 110 R. Huang, L. He, T. Zhang, D. Li, P. Tang and Y. Feng, *ACS Appl. Mater. Interfaces*, 2018, **10**, 22776–22785.
- 111 L. Sun, Y. Tian, J. Zhang, W. Hao Cui and J. L. Zuo, *Chem. Eng. J.*, 2018, **344**, 246–253.
- 112 L. Sun, Y. Tian, J. Zhang, H. Li, C. Tang and J. Lia, *Chem. Eng. J.*, 2018, **343**, 455–459.
- 113 Y. Huang, J. Tang, L. Gai, Y. Gong, H. Guan, R. He and H. Lyu, *Chem. Eng. J.*, 2017, **319**, 229–239.

